HHS Public Access

Author manuscript

Magn Reson Med. Author manuscript; available in PMC 2022 June 01.

Published in final edited form as:

Magn Reson Med. 2021 June ; 85(6): 3383–3393. doi:10.1002/mrm.28668.

BULK VOLUME SUSCEPTIBILITY DIFFERENCE BETWEEN DEOXYHEMOGLOBIN AND OXYHEMOGLOBIN FOR HbA AND HbS: A COMPARATIVE STUDY

Cihat Eldeniz[1], **Michael M Binkley**[2], **Melanie Fields**[3], **Kristin Guilliams**[2,3], **Dustin K Ragan**[4], **Yasheng Chen**[2], **Jin-Moo Lee**[1,2,5], **Andria L Ford**[1,2], **Hongyu An**[1,2,5]

[1]Mallinckrodt Institute of Radiology, Washington University in St. Louis, St. Louis, Missouri, USA

[2]Department of Neurology, Washington University in St. Louis, St. Louis, Missouri, USA

[3]Department of Pediatrics, Washington University in St. Louis, St. Louis, Missouri, USA

[4]Department of Radiology, Medical College of Wisconsin, Milwaukee, Wisconsin, USA

[5]Department of Biomedical Engineering, Washington University in St. Louis, St. Louis, Missouri, USA

Abstract

Purpose: Sickle cell anemia (SCA) is a blood disorder that alters the morphology and the oxygen affinity of the red blood cells. Cerebral oxygen extraction fraction (OEF) measurements using quantitative blood oxygenation level dependent (BOLD) contrast have been employed for assessing inadequate oxygen delivery and the subsequent risk of ischemic stroke in SCA. The BOLD signal in magnetic resonance imaging (MRI) studies relies on $\Delta\chi_{do}$, the bulk volume susceptibility difference between fully oxygenated and fully deoxygenated blood. Several studies have measured $\Delta\chi_{do}$ for normal hemoglobin (HbA). However, it is not known if the value is different for sickle hemoglobin (HbS). In this study, $\Delta\chi_{do}$ was measured for both HbA and HbS.

Methods: Six SCA patients and six controls were recruited. Various blood oxygenation levels were achieved via in vivo manipulations to keep the blood close to its natural state. To account for the differences in oxygen affinity, Hill's equations were used to translate partial pressure of oxygen to oxygen saturation for HbA, HbS and HbF separately. pH and PCO_2 corrections were performed. Temperature and magnetic field drift were controlled for. A multivariate generalized linear mixed model with random participant effect was employed.

Results: Assuming that $\Delta\chi_{do}$ is similar for HbA and HbF and that $\Delta\chi_{metHb}$ is 5/4 of $\Delta\chi_{do}$ for HbA, it was found that the $\Delta\chi_{do}$ values for HbA and HbS were not statistically significantly different from each other.

Conclusion: The same $\Delta\chi_{do}$ value can be used for both types of hemoglobin in quantitative BOLD analysis.

Corresponding author: Hongyu An, DSc, Mallinckrodt Institute of Radiology, Washington University School of Medicine, 510 S Kingshighway, WPAV CCIR, CB 8131, St. Louis, MO 63110, hongyuan@wustl.edu.

Keywords

magnetic susceptibility; sickle cell disease; blood

Introduction

Sickle cell anemia (SCA) is an inherited blood disorder which leads to lifelong disability and early mortality (1). Hemoglobin (Hb) is a tetrameric protein in red blood cells (RBC) that is responsible for carrying oxygen from the lungs to the whole body. SCA is caused by a genetic mutation that changes hemoglobin A (HbA) to abnormal sickle hemoglobin (HbS) (2). HbA consists of two α- and two β-globin chains ($\alpha_2\beta_2$)(3), and comprises 97% of the hemoglobin in healthy adult blood. The dominant hemoglobin in patients with SCA, however, is HbS, ($\alpha_2\beta_2^S$), where β^S is a qualitatively abnormal β-globin that results from a single base pair mutation in the sixth codon of the β-globin gene, substituting valine for glutamic acid (4,5). Upon deoxygenation, HbS aggregates and polymerizes, leading to the morphological deformation, or sickling, of the red blood cells (6,7). This polymerization reduces the oxygen affinity of HbS under hypoxic conditions, with the amount of reduction depending on the severity of polymerization (8,9). Fetal hemoglobin (HbF), on the other hand, contains two α- and two γ-globin chains ($\alpha_2\gamma_2$) (10). The percentage of HbF in blood normally decreases to less than 1% during the first two years after birth, but may persist in adults with certain disorders. The percentage of HbF can reach approximately 30% in patients with SCA (11). HbA, HbF, and HbS can all bind oxygen, albeit with different oxygen affinities. However, hemoglobin cannot bind oxygen if the iron in the heme group is in the ferric state (Fe^{+3}) rather than in the ferrous state (Fe^{+2}), termed methemoglobin (MetHb); or when carbon monoxide is bound, termed carboxyhemoglobin (COHb). In SCA, the levels of MetHb and COHb are elevated due to intravascular hemolysis, compared to those that are unaffected (12).

In their seminal work, Pauling and Coryell demonstrated that oxygen-carrying hemoglobin (OxyHb) and COHb contain no unpaired electrons, while deoxyhemoglobin (DeoxyHb) has 4 unpaired electrons per heme. As a result, both OxyHb and COHb are diamagnetic, while DeoxyHb is paramagnetic (13). The discovery that DeoxyHb is paramagnetic has led to the development of blood oxygenation level-dependent (BOLD) contrast in MRI (14). The BOLD signal can be used to monitor cerebral hemodynamic alterations due to brain activity (15,16), and to quantify tissue hemodynamic parameters such as oxygen extraction fraction (OEF) (17–19). Additionally, Coryell *et al.* have found that MetHb is paramagnetic with 5 unpaired electrons per heme(20). In SCA, there has been great interest in the measurement of tissue-level cerebral OEF as an index of hypoxia-ischemia due to chronic anemia and subsequent risk of ischemic stroke (21–24). In this respect, quantitatively measured alterations in cerebral oxygenation using BOLD contrast may provide insight into tissue vulnerability in SCA (21,22,25). This quantitation, however, requires the knowledge of the bulk volume susceptibility difference between fully oxygenated blood and fully deoxygenated blood, which is denoted as $\Delta\chi_{do}$.

Magnetic susceptibility (χ) is a proportionality constant that governs the amount of magnetization induced in an object by an external field, while bulk volume susceptibility (χ_b) is the average of this effect throughout the whole volume of the object. Measuring $\Delta\ \chi_{do}$ involves the measurement of bulk volume susceptibility, χ_b, of blood at various oxygenation levels.

A number of studies have examined $\Delta\ \chi_{do}$ for HbA. Thulborn *et al.* made use of blood samples drawn from rats and rabbits, and arrived at $\Delta\ \chi_{do}$ = 0.2 ppm in cgs units (26). Weisskoff and Kiihne found $\Delta\ \chi_{do}$ = 0.18 [cgs, ppm] by imaging expired human whole blood or packed red cells obtained from the hospital blood bank, with an asymmetric spin-echo echo-planar imaging (EPI) sequence(27). Spees *et al.*(28) obtained $\Delta\ \chi_{do}$ = 0.27 [cgs, ppm] by using a spin-echo-based spectroscopy sequence. This value was later confirmed by Jain *et al.* (29) who found $\Delta\ \chi_{do}$ = 0.273 [cgs, ppm] by using the phase images obtained from a double-echo gradient-echo (GRE) sequence. In all of the studies mentioned above (26–29), various oxygenation levels were obtained by in vitro manipulation of blood.

Studies to date have measured $\Delta\ \chi_{do}$ for HbA only. However, it is unknown whether the value of $\Delta\ \chi_{do}$ for HbS differs from that for HbA. This study measures $\Delta\ \chi_{do}$ for both HbA and HbS by using blood from healthy participants and SCA patients. Furthermore, to evaluate bulk volume susceptibility variations across a range of physiological blood oxygen levels, we manipulated oxygenation in vivo, rather than in vitro, so as to keep the blood as close as possible to its natural state. Moreover, previously published oxygen dissociation curves were used for deriving isoform-specific sO_2 values for a more accurate DeoxyHb calculation. In addition, $P50$ was adjusted based on the pH and PCO_2 measurements in each blood sample. Finally, we measured $\Delta\ \chi_{do}$ after controlling for factors known to affect the susceptibility measurements such as magnetic field drift and temperature.

Methods

Blood Preparation

The study was approved by the Institutional Review Board (IRB). Six SCA patients (age range 28.3±9.4, 3 females) and six healthy volunteers (with no kinship with the patients, age range 38.2±9.8, median age was not statistically significantly different from that for the SCA patients, Wilcoxon rank sum test P=0.17, 2 females) were recruited with informed consent. No participant was excluded from the data analysis. For each participant, venous blood was drawn from the antecubital vein into heparinized tubes at four different oxygenation conditions: [1] normoxemia, [2] hypoxemia (due to ischemia), [3] recovery to normoxemia, and [4] hyperoxemia (hyperoxia). We achieved the reduced and elevated blood oxygenation levels in vivo, rather than in vitro, in order to minimize the potential damage to red blood cells. For Condition 1 (baseline), participants breathed ambient air. For Condition 2 (ischemia), a tourniquet was applied about 3–4 inches above the antecubital vein on one of the arms and the participants exercised the hand on the same side by squeezing a ball for up to three minutes to achieve a reduced-oxygenation state. We removed the tourniquet after blood sampling. The samples for Condition 3 (recovery after hypoxia) were collected after

10 minutes of breathing room air. For Condition 4 (hyperoxemia), the participants breathed 100% oxygen through a simple face mask for 10 minutes. Two 3-mL samples were drawn at the end of each blood oxygenation condition. The first blood sample was immediately hand-carried to the hospital's CLIA-certified laboratory in an approximately 37-degree-Celsius water bath for co-oximetry, venous blood oxygen saturation measurements (sO_2), and hemoglobin analysis for quantification of hemoglobin isoforms. The second blood sample was used for MR imaging. The air bubbles in the sample were removed as quickly as possible and the sample was then kept in a 37.5°C water bath for 3 minutes prior to imaging.

A custom phantom holder made of thermally insulating styrofoam minimized the cooling of the blood sample in the scanner (Figure 1). To examine the effectiveness of temperature insulation, we used a fiber-optic temperature probe placed inside two distilled water samples – one kept inside, one kept outside the phantom holder, and measured the temperature as a function of time.

MR Imaging

All imaging was performed on a 3T Siemens mMR Biograph scanner. Two 4-channel carotid artery coils were used for imaging – one at the top and one at the bottom of the phantom holder, which was carefully placed so that the long axis of the five syringes would be parallel to B_o. Five syringes filled with distilled water at room temperature were first scanned to perform frequency adjustment and shimming. Next, the blood sample was transported from the water bath to the scanner (3 meters walk) in a warm towel. During the transportation, the blood sample syringe was gently rotated so that the red blood cells would be mixed well with the plasma. The blood sample syringe was then placed at the center, replacing the middle syringe, while the other 4 water syringes were kept in place.

An 8-echo GRE sequence with monopolar readout was used to obtain the susceptibility measurements with the following imaging parameters: TR=40 ms. TE(i)=3.36+(i-1)*4.55 ms for i = 1,2,…,8, Matrix size = 192×54, single slice, voxel size = 0.75×0.75×5 mm. The acquisition time of the GRE sequence was 2.5 seconds. The total time from the blood sample leaving the water bath to the completion of the GRE scan was less than 30 seconds.

Susceptibility Measurements

The complex phase of the signal collected by Coil element c at any given voxel can be described as follows (30):

$$\begin{aligned}\varnothing_c(x,y,z,TE) &= \varnothing_{o,c} - \gamma \cdot \Delta B(x,y,z) \cdot TE \\ &= \varnothing_{o,c} - \gamma \cdot \left[\frac{4\pi}{6}\left(3cos^2\theta - 1\right)\chi_b(x,y,z) \cdot B_o\right] \cdot TE \\ &= \varnothing_{o,c} - \gamma \cdot \frac{4\pi}{3}\chi_b(x,y,z) \cdot B_o \cdot TE\end{aligned} \quad [1]$$

where $\varnothing_{o,c}$ is the baseline phase-offset for Coil element c, γ is the gyromagnetic ratio, $\theta = 0$ is the angle the syringes make with the z-axis, $\chi_b(x,y,z)$ is the bulk volume susceptibility value for the voxel located at (x,y,z), B_o is the magnetic field strength of the scanner and TE is the echo time. The complex images from multiple coils were combined for obtaining

phase images with high signal-to-noise-ratio (SNR) that would be used for estimating χ_b. Since $\varnothing_{o,c}$ varies from coil element to coil element, a simple complex summation can lead to signal loss due to phase cancellation. To overcome this problem, phase images were obtained as follows(31):

- For each element of the receiver coil, the multi-echo phase data was first unwrapped across echo times, and then a linear regression was applied to obtain the intercept value, $\varnothing_{o,c}$.
- The coil-specific intercept was subtracted from the phase data of each individual coil element.
- The phase images were then computed as the phase of the complex sum of these phase-aligned coil element data.

In order to obtain the bulk volume susceptibilities, χ_b, on a per-voxel basis, the images were processed as follows:

- The combined phases were unwrapped across echo times.
- The combined magnitude images were smoothed with a 2.25×2.25-mm kernel.
- A weighted linear least-squares fit was applied to the unwrapped phase to estimate χ_b. The weight used for each echo was the square of the smoothed magnitude value for that echo since the variance of the phase noise is inversely proportional to magnitude for large-SNR regions(32). The first echo was masked with a threshold equal to 7 background noise standard deviations. The later echoes were also excluded from the least-squares fitting if the signal dropped below one fifth of this threshold.
- Over time, the main magnetic field may drift. To account for this drift, the average susceptibility of the distilled water syringes on the two sides of the blood sample was used as a reference since the bulk volume susceptibilities of these syringes were expected to be constant over time. Any changes in this average bulk volume susceptibility was considered to be caused by magnetic field drift and was subtracted from the bulk volume susceptibility measured in the blood sample.

Controlling for temperature

Air bubble removal could take 30–40 seconds in some cases, potentially leading to changes in temperature. For this reason, we examined whether keeping the sample for 3 minutes inside the water bath was sufficient to reach the desired temperature after air bubble removal. Temperature measurement was performed in 3 distilled water samples that simulated air bubble removal times of 0, 30 and 60 sec. Moreover, considering the importance of temperature on susceptibility(33), the bulk volume susceptibility of a water sample was measured in a separate experiment as a function of temperature values covering body temperature and ambient temperature inside the scanner room. The difference between the susceptibility of water at body temperature and the room temperature was then used for correcting the offset in the susceptibility measurements.

Bulk Volume Susceptibility of Various Hemoglobin Isoforms

DeoxyHb and MetHb are paramagnetic, and hence contribute to the overall susceptibility, χ_b, measured in the blood. In this respect, χ_b can be expressed as:

$$\chi_b = Q_A \, \Delta \, \chi_{do,A} + Q_F \, \Delta \, \chi_{do,F} + Q_S \, \Delta \, \chi_{do,S} + Q_M \, \Delta \, \chi_{met} + \alpha_0 \quad [2]$$

where

$$Q_A = Hct(1 - COHb - MetHb)\, r_A \left(1 - sO_{2,A}\right)$$

$$Q_F = Hct(1 - COHb - MetHb)\, r_F \left(1 - sO_{2,F}\right)$$

$$Q_S = Hct\,(1 - COHb - MetHb)\, r_S \left(1 - sO_{2,S}\right)$$

$$Q_M = Hct\; MetHb$$

and α_0 is the intercept of the linear model. Here, $\Delta \chi_{do,A}$, $\Delta \chi_{do,F}$ and $\Delta \chi_{do,S}$ are the bulk volume susceptibility differences between fully oxygenated and fully deoxygenated HbA, HbF and HbS, respectively. Hct is the hematocrit level. $sO_{2,A}, sO_{2,F}$ and $sO_{2,S}$ are the oxygen saturation fractions of HbA, HbF and HbS, respectively. $COHb$ and $MetHb$ are the fractions of COHb and MetHb out of all hemoglobins, in respective order. r_A, r_F and r_S are the "protein-based fractions" of HbA, HbF and HbS, respectively, with $r_A + r_F + r_S = 1$. According to these definitions, $(1 - COHb - MetHb)$ is the fraction of functional hemoglobin that can bind oxygen, regardless of the isoform (A, F or S).

sO_2 derived from PO_2 using oxygen dissociation curves

Please note that the sO_2 values provided by the co-oximetry were ratios between oxygenated Hb and total Hb, regardless of the hemoglobin isoform. Given that HbA, HbF and HbS have different oxygen affinities (34,35), the co-oximetry-provided sO_2 values cannot be simply distributed in proportion to the percentages of these hemoglobins to obtain $sO_{2,A}, sO_{2,F}$ and $sO_{2,S}$. In order to overcome this issue, for each sample, the partial pressure of oxygen in the blood, PO_2, and the oxygen dissociation curves specific to each hemoglobin isoform were employed to obtain the oxygen saturation fractions sO_2 based on Hill's equation:

$$\boldsymbol{sO}_2 = (PO_2/P50)^n / \left(1 + (PO_2/P50)^n\right) \quad [3]$$

where n is the Hill coefficient, $P50$ is the value of PO_2 at 50% oxygen saturation.

For HbA, n=2.7 and $P50$=26.8 were used based on the results reported by Dash et al. (36). The cord blood oxygen dissociation curve published by Maurer *et al.* (34) was used to fit Hill's equation to obtain n and $P50$ for HbF. Finally, the sickle cell oxygen dissociation curves reported by Becklake *et al.* (35) and Wagner *et al.* (37) were used to derive the parameters of Hill's equation for HbS as two alternative models. Given that $P50$ is a function of pH, PCO2, and 2,3-DPG, we implemented the $P50$ correction via Equations 9 and 10 in Dash et al.(36). Since 2,3-DPG was not measured in this study, its effect on $P50$ was not accounted for. The values of $sO_{2,A}$, $sO_{2,F}$ and $sO_{2,S}$ derived via Equation 3 were substituted into Equations 2 and 4. The model using Becklake et al.'s HbS curve was termed as Dash-Becklake-Maurer (DBM), while the model using Wagner et al.'s HbS curve was termed as Dash-Wagner-Maurer (DWM). In order to examine how well these models would represent the measured data, the derived oxygen saturation values were weighted by the fraction of each hemoglobin isoform, and the sum of these values was then compared with the overall oxygen saturation values provided by the co-oximetry for each blood sample.

Reduced models

Since there were multiple blood samples at different oxygenation levels from each participant, a multivariate generalized linear mixed model with random participant effect was employed using all data from both controls and SCA patients. Considering that the fractions of HbF were much smaller than those of HbA and HbS (Table 1), we combined HbA and HbF in the statistical analysis with the assumption that HbA and HbF have similar $\Delta\chi_{do}$ values. Moreover, since MetHb has 5 unpaired electrons per heme, while deoxygenated HbA has 4 unpaired electrons (20), we assumed that $\Delta\chi_{met}$ is $\frac{5}{4}\Delta\chi_{do,AF}$. This way, the number of independent variables was reduced, increasing the statistical power. Here is the reduced model:

$$\chi_b = \left(Q_A + Q_F + \frac{5}{4}Q_M\right)\Delta\chi_{do,AF} + Q_S\,\Delta\chi_{do,S} + \alpha_0 \quad [4]$$

assuming that $\Delta\chi_{do,AF} \approx \Delta\chi_{do,A} \approx \Delta\chi_{do,F}$.

The independent variables included in the multivariate model were deoxygenated (HbA +HbF) and deoxygenated HbS, with a type I error rate of 0.05 for determining the regression coefficients and overall model significance. Possible interaction between the clinical predictors was statistically assessed.

To compare the value of $\Delta\chi_{do,A}$ measured in this study to those reported in the literature, a separate linear mixed model with random participant-specific effect was fitted using healthy controls only:

$$\chi_b = \left(Q_A + \frac{5}{4}Q_M\right)\Delta\chi_{do,A} + \alpha_0 \quad [5]$$

The empirical difference between $\Delta\chi_{do,AF}$ and $\Delta\chi_{do,S}$ was tested using the regression coefficients from the multivariate linear mixed model, parameter variance, and parameter

covariance with a two-sided significance threshold of 0.05. For a z-score greater than 1.96, the null hypothesis, H_0: $\Delta\chi_{do,AF} = \Delta\chi_{do,S}$, will be rejected. Akaike information criterion (AIC) were computed for both the DBM and DWM models. Difference in modeled values for susceptibility and observed values were analyzed with a linear regression using R^2 for goodness-of-fit.

Results

Participant Characteristics

Table 1 lists the participant characteristics and blood analysis results.

Drift in imaging frequency

With the imaging frequency being about 123.21 MHz, the drift in the imaging frequency measured via the reference distilled water syringes ranged from −4.88 Hz to 1.15 Hz across all samples collected from all participants. The per-participant frequency difference between the most deoxygenated and the most oxygenated states in blood ranged from 1.68 to 7.65 Hz, whereas the per-participant frequency drifts in the reference distilled water syringes ranged from 0.22 to 2.89 Hz, which demonstrated that the magnetic field drifts over time were not negligible and accounting for the drift was essential.

Sample Temperature Control

After two water syringes at an initial temperature of 37.5°C were allowed to cool down by being exposed to room temperature for 30 seconds and 60 seconds, respectively, and then placed in the water bath maintained at 37.5 ± 0.5 °C, it took about 30 seconds and 70 seconds, in respective order, for the samples to reach a steady-state within the target temperature range of 37.5 ± 0.5 °C. Therefore, as an extreme example, even if the removal of the air bubbles lasted for up to 70 seconds, 3 minutes of water bath immersion was found to be sufficient to stabilize the temperature of the blood samples.

Figure 2 shows the temperature decrease in the syringes with and without foam insulation after they left the water bath. This figure plots the discrete measurements collected every 30 seconds, as well as the following exponential function used for estimating the temperature decay constant, τ:

$$T(t) = T_f + \left(T_i - T_f\right)e^{-t/\tau} \quad [6]$$

where T_i is the initial temperature, T_f is the room temperature and τ is the decay constant. This plot suggests that the insulating foam decreases the decay constant approximately by half. For example, a sample at 37.5°C cools down by 0.47°C inside the foam holder after 30 seconds (i.e. the total measurement time inside the scanner), while it cools down by 0.92°C in the absence of the holder.

The dependence of bulk volume susceptibility on temperature

As Figure 3 depicts, the relationship between bulk volume susceptibility and temperature is mostly linear within the temperature range of interest. According to this figure, the change in

bulk volume susceptibility is expected to be about 2.6×10^{-3} ppm in cgs units for an estimated decrease of 1°C in temperature. While this is negligible when compared with the levels of bulk volume susceptibility variations due to various oxygenation levels of the blood, we minimized sample heat loss using identical methods in both controls and patients.

sO_2 derived from PO_2 using oxygen dissociation curves

Based on Maurer *et al.*'s data for HbF, the fitted parameters of the Hill equation were n=3 and $P50$=20. The parameters for Becklake *et al.*'s HbS curve were n=2.55 and $P50$=32 for HbS, while they were n=3 and $P50$=40 for Wagner *et al.*'s HbS curve.

Figure 4 examines how well the weighted sum of the sO_2 values obtained from literature (as mentioned in the Methods section) agrees with the co-oximetry-measured sO_2 values. For both the DBM (Figure 4a) and the DWM (Figure 4b) models, the points are clustered around the identity line (green line), with few outliers. The regression coefficient for these points and the corresponding 95% confidence interval for the DBM model were 0.9981 (0.9707,1.0255) with an R^2 value of 0.8500, while the statistics for the DWM model were 1.0301 (1.0003,1.0600) with an R^2 value of 0.8330. Both regressions showed good agreement between the modeled (weighted sum) vs. measured oxygen saturation.

Bulk volume susceptibility difference measurements using the reduced models

For the DBM model, the estimated values of $\Delta\chi_{do,AF}$ and $\Delta\chi_{do,S}$ (and their 95% confidence intervals) were 0.195 (0.159, 0.230) [cgs, ppm] and 0.274 (0.174, 0.373) [cgs, ppm] for (HbA+HbF) and HbS, respectively, with an R^2 value of 0.827. $\Delta\chi_{do,AF}$ and $\Delta\chi_{do,S}$ were not statistically different from each other (P=0.121). For the DWM model, the estimated values of $\Delta\chi_{do,AF}$ and $\Delta\chi_{do,S}$, and their 95% confidence intervals were 0.197 (0.162, 0.232) [cgs, ppm] and 0.225 (0.146, 0.304) [cgs, ppm] for HbA+HbF and HbS, respectively, with an R^2 value of 0.831. $\Delta\chi_{do,AF}$ and $\Delta\chi_{do,S}$ were not significantly different from each other (P=0.490), which is consistent with the conclusion obtained by using the DBM model. The AIC were computed as −307.3 and −308.1 for the DBM and DWM models, respectively.

In the analysis of the data obtained from the control group, $\Delta\chi_{do,A}$ in Equation 5 was found to be 0.193 (0.154, 0.234) [cgs, ppm] with random participant effect. The excellent agreement between the $\Delta\chi_{do,AF}$ value estimated from all participants using Equation 4 and the $\Delta\chi_{do,A}$ value estimated only from the healthy controls using Equation 5 suggests that our $\Delta\chi_{do,A}$ measurements are highly reliable.

Figure 5 demonstrates the measured and modeled susceptibilities using the DBM and DWM models.

Sensitivity Analysis

Estimation of the effect of unknown temperature variability on the regression coefficients from the reported mixed model ($\chi_b = (Q_A + Q_F + \frac{5}{4}Q_M)\Delta\chi_{do,AF} + Q_S\Delta\chi_{do,S} + \alpha_0$) for the DBM and DWM datasets indicated non-significant changes in the regression coefficients for $\Delta\chi_{do,AF}$ (p=0.967 and p=0.958, respectively) and $\Delta\chi_{do,S}$ (p=0.939 and p=0.931, respectively). This was estimated using a modified bootstrap that introduced statistical noise (μ=0°C, σ=0.3°C) to the measured susceptibility over 500 iterations assuming a slope of 0.0026 ppm/°C. Variability attributed to temperature change represents on average a 1.8% (1.4%, 2.2%) of the patient specific variability accounted for within the model.

Discussion and Conclusions

The bulk volume susceptibility difference between deoxygenated and oxygenated hemoglobin, $\Delta\chi_{do}$, provides the basis for the calculation of OEF using quantitative BOLD methods (17,19,38). OEF measurements are of great clinical interest in SCA where low blood oxygen content due to anemia and other downstream disease mechanisms lead to inadequate oxygen supply to meet tissues' metabolic demands. Various hemoglobin isoforms including HbA, HbS, and HbF co-exist in the blood of SCA patients. Moreover, the fractions of COHb and MetHb are elevated in SCA. DeoxyHb and MetHb are paramagnetic, while OxyHb and COHb are diamagnetic. To ensure accurate OEF measurements in SCA patients, it is important to measure $\Delta\chi_{do}$ of various hemoglobins that contribute to the overall bulk volume susceptibility. Due to their different oxygen affinities, the oxygen saturation values for a given PO_2 level are different among HbA, HbS and HbF. In this study, we accounted for the distinct bulk volume susceptibility differences of these hemoglobins as indicated in Equation 2. We assumed that the bulk volume susceptibility differences were similar between DeoxyHbA and DeoxyHbF, and that MetHb's susceptibility was 5/4 higher than that of DeoxyHbA; thus, we estimated $\Delta\chi_{do}$ for HbA and HbS only. Our findings suggest that $\Delta\chi_{do,A}$ and $\Delta\chi_{do,S}$ are not statistically different, implying that a single $\Delta\chi_{do}$ value can be used for both HbA and HbS to measure OEF in SCA using a quantitative BOLD method. To the best of our knowledge, our study is the first to investigate $\Delta\chi_{do}$ for the human HbS.

Our study has several strengths which add confidence to our findings: 1) All blood oxygenation manipulations were performed in vivo using simple maneuvers (exercising, oxygen breathing), keeping the blood cells as intact as possible, 2) The temperature of the blood samples were carefully controlled and the temperature-dependent change in the susceptibility of water was taken into account; 3) The temporal drift in the magnetic field was corrected using the two water samples placed next to the blood sample to serve as reference; 4) Given the partial pressure of oxygen recorded for each blood sample, oxygen saturation values were obtained for each hemoglobin isoform by using the oxygen dissociation curve particular to that hemoglobin isoform; 5) $P50$ was corrected based on the pH and PCO_2 measurements in each blood sample; 6) We measured $\Delta\chi_{do,A}$ for all participants and also for healthy controls only. The agreement between the two

measurements of $\Delta\chi_{do,A}$ further supports the accuracy of our findings. Several bulk volume susceptibility results have been reported for HbA. Reported values include: = 0.18 [cgs, ppm] (27), 0.2 [cgs, ppm] (26) and 0.27 [cgs, ppm] (28),(29). In the current study, we found $\Delta\chi_{do,A}$ = 0.193 (0.154, 0.234) [cgs, ppm]. Our value for $\Delta\chi_{do,A}$ fall within the 95% confidence interval of two previous studies (26,27), however, our values fall outside of values reported in two other studies (28,29). A number of factors might have led to this discrepancy. First, our blood samples were scanned within minutes of being drawn as opposed to being stored for use within 24 hours (28) or 6 hours (29). Therefore, the blood was fresh and closest to its in vivo state. Second, the GRE acquisition in our study took only 2.5 seconds, minimizing blood cell aggregation. For this reason, the samples did not need to be tumbled as in (28) and (29), which minimized potential damage to the blood cells. Third, in contrast with (28), our blood samples were not diluted with human plasma. Finally, to the best of our knowledge, in all of the prior published studies, various blood oxygenation levels were always achieved by in vitro manipulation such as exposure to gases, while oxygenation alteration was achieved in vivo in our study. Our experimental setup therefore imposes the least risk of artificially altering red blood cells.

In this study, three oxygen dissociation curves were used to derive HbA-, HbS-, and HbF-specific sO_2 values from PO_2 values. There are very few studies in the literature that provide oxygen dissociation curves for HbS and HbF. Maurer et al.(34) published the oxygen dissociation curve for HbF using the cord blood, while Becklake *et al.*(35) and Wagner *et al.* (37) reported oxygen dissociation curves for HbS. 4 SCA patients were studied in Becklake et al. compared to 1 patient in Wagner et al. There is a recent study published by Young *et al.* on oxygen dissociation for HbS that used data from 45 patients (39). We found conflicting results in Young et al.'s paper (more specifically, Table 1 vs. Figure 1). In addition, the model constructed by using Hill's equation parameters for HbA, HbS and HbF in Young's study, which we will refer to as the "YYY" model in what follows, has lower AIC (AIC= −305.5) than that of the DBM model (AIC=−307.3) and the DWM model (AIC=−308.1). It is only 0.27 times as probable for the YYY model to minimize the information loss when compared with the DWM model. Moreover, the YYY model did not fit the experimental data as well as the DBM and DWM models did – the R^2 value for the YYY model (0.821) was lower than those for both the DBM (0.827) and the DWM (0.831) models. Therefore, we decided not to include the results from the YYY model. Despite the difference in the modeling of the HbS dissociation curve between the DBM and the DWM models, $\Delta\chi_{do,AF}$ and $\Delta\chi_{do,S}$ were not significantly different from each other in both models.

There are limitations in this study. First, 2,3-diphosphoglycerate (2,3-DPG) may affect the oxygen affinity of the hemoglobins (36,40,41). However, 2,3-DPG was not measured in this study protocol. Therefore, its effect was not accounted for. Second, at low oxygenation levels, HbS may polymerize, potentially leading to variabilities in the $\Delta\chi_{do,S}$ values across low and high oxygenation levels. We were unable to account for the impact of HbS polymerization as noninvasive means to measure polymerization do not exist. Finally, the current sample size was inadequate to investigate interaction effects between HbA and HbS within SCA patients. A larger sample size would allow for the assessment of within-subject,

between-subject, and between-cohort variability of HbS and HbA, thereby providing more accurate parameter estimates.

In conclusion, the volume susceptibility of HbS is not statistically different from that of HbA. Our findings lay the groundwork for quantitative BOLD and voxel-wise OEF measurements in SCA patients.

Acknowledgments

The authors would like to thank Liam Comiskey for helping with the patient recruitment and logistic support and would also like to acknowledge the following funding sources: NIH 1R01NS082561, NIH 1RF1NS116565, 1P30NS098577, 2R01HL129241, R01NS085419, U24NS107230, K23HL136904 (NHLBI) and K23NS099472. This manuscript was edited by the Scientific Editing Service of the Institute of Clinical and Translational Sciences at Washington University, which is supported by an NIH Clinical and Translational Science Award (UL1 TR002345).

References

1. Ware RE, de Montalembert M, Tshilolo L, Abboud MR. Sickle cell disease. Lancet Lond. Engl 2017;390:311–323.
2. Yonetani T, Laberge M. Protein Dynamics Explain the Allosteric Behaviors of Hemoglobin. Biochim. Biophys. Acta 2008;1784:1146–1158. [PubMed: 18519045]
3. Schnog JB, Duits AJ, Muskiet F a. J, ten Cate H, Rojer RA, Brandjes DPM. Sickle cell disease; a general overview. Neth. J. Med 2004;62:364–374. [PubMed: 15683091]
4. Pauling L, Itano HA. Sickle cell anemia a molecular disease. Science 1949;110:543–548. [PubMed: 15395398]
5. Marotta CA, Wilson JT, Forget BG, Weissman SM. Human beta-globin messenger RNA. III. Nucleotide sequences derived from complementary DNA. J. Biol. Chem 1977;252:5040–5053. [PubMed: 68958]
6. Dean J, Schechter AN. Sickle-Cell Anemia: Molecular and Cellular Bases of Therapeutic Approaches. N. Engl. J. Med 1978;299:752–763. [PubMed: 357967]
7. Bunn HF. Pathogenesis and Treatment of Sickle Cell Disease. N. Engl. J. Med 1997;337:762–769. [PubMed: 9287233]
8. Benesch RE, Edalji R, Kwong S, Benesch R. Oxygen affinity as an index of hemoglobin S polymerization: A new micromethod. Anal. Biochem 1978;89:162–173. [PubMed: 30335]
9. Abdu A, Gómez-Márquez J, Aldrich TK. The oxygen affinity of sickle hemoglobin. Respir. Physiol. Neurobiol 2008;161:92–94. [PubMed: 18249588]
10. Von Krueger F Ueber die ungleiche Resistenz des Blutfarbstoffs verschiedener Thiere gegen zersetzende Agentien. Z Biol 24:318–335.
11. Rochette J, Craig JE, Thein SL, Rochette J. Fetal hemoglobin levels in adults. Blood Rev. 1994;8:213–224. [PubMed: 7534152]
12. Caboot JB, Jawad AF, McDonough JM, et al. Non-Invasive Measurements of Carboxyhemoglobin and Methemoglobin in Children with Sickle Cell Disease. Pediatr. Pulmonol 2012;47:808–815. [PubMed: 22328189]
13. Pauling L, Coryell CD. The Magnetic Properties and Structure of Hemoglobin, Oxyhemoglobin and Carbonmonoxyhemoglobin. Proc. Natl. Acad. Sci. U. S. A 1936;22:210–216. [PubMed: 16577697]
14. Ogawa S, Lee TM, Kay AR, Tank DW. Brain magnetic resonance imaging with contrast dependent on blood oxygenation. Proc. Natl. Acad. Sci. U. S. A 1990;87:9868–9872. [PubMed: 2124706]
15. Bandettini PA, Wong EC, Hinks RS, Tikofsky RS, Hyde JS. Time course EPI of human brain function during task activation. Magn. Reson. Med 1992;25:390–397. [PubMed: 1614324]

16. Kwong KK, Belliveau JW, Chesler DA, et al. Dynamic magnetic resonance imaging of human brain activity during primary sensory stimulation. Proc. Natl. Acad. Sci. U. S. A 1992;89:5675–5679. [PubMed: 1608978]
17. An H, Lin W. Quantitative measurements of cerebral blood oxygen saturation using magnetic resonance imaging. J. Cereb. Blood Flow Metab. Off. J. Int. Soc. Cereb. Blood Flow Metab 2000;20:1225–1236.
18. An H, Lin W. Impact of intravascular signal on quantitative measures of cerebral oxygen extraction and blood volume under normo- and hypercapnic conditions using an asymmetric spin echo approach. Magn. Reson. Med 2003;50:708–716. [PubMed: 14523956]
19. He X, Yablonskiy DA. Quantitative BOLD: Mapping of human cerebral deoxygenated blood volume and oxygen extraction fraction: Default state. Magn. Reson. Med 2007;57:115–126. [PubMed: 17191227]
20. Coryell CD, Stitt F, Pauling L. The Magnetic Properties and Structure of Ferrihemoglobin (Methemoglobin) and Some of its Compounds. J. Am. Chem. Soc 1937;59:633–642.
21. Fields ME, Guilliams KP, Ragan DK, et al. Regional oxygen extraction predicts border zone vulnerability to stroke in sickle cell disease. Neurology 2018;90:e1134–e1142. [PubMed: 29500287]
22. Guilliams KP, Fields ME, Ragan DK, et al. Red cell exchange transfusions lower cerebral blood flow and oxygen extraction fraction in pediatric sickle cell anemia. Blood 2018;131:1012. [PubMed: 29255068]
23. Jordan LC, Gindville MC, Scott AO, et al. Non-invasive imaging of oxygen extraction fraction in adults with sickle cell anaemia. Brain J. Neurol 2016;139:738–750.
24. Bush AM, Coates TD, Wood JC. Diminished cerebral oxygen extraction and metabolic rate in sickle cell disease using T2 relaxation under spin tagging MRI. Magn. Reson. Med. 2018;80:294–303. [PubMed: 29194727]
25. Fields ME, Guilliams KP, Ragan D, et al. Hydroxyurea reduces cerebral metabolic stress in patients with sickle cell anemia. Blood 2019.
26. Thulborn KR, Waterton JC, Matthews PM, Radda GK. Oxygenation dependence of the transverse relaxation time of water protons in whole blood at high field. Biochim. Biophys. Acta 1982;714:265–270. [PubMed: 6275909]
27. Weisskoff RM, Kiihne S. MRI susceptometry: image-based measurement of absolute susceptibility of MR contrast agents and human blood. Magn. Reson. Med 1992;24:375–383. [PubMed: 1569876]
28. Spees WM, Yablonskiy DA, Oswood MC, Ackerman JJ. Water proton MR properties of human blood at 1.5 Tesla: magnetic susceptibility, T(1), T(2), T*(2), and non-Lorentzian signal behavior. Magn. Reson. Med 2001;45:533–542. [PubMed: 11283978]
29. Jain V, Abdulmalik O, Propert KJ, Wehrli FW. Investigating the magnetic susceptibility properties of fresh human blood for noninvasive oxygen saturation quantification. Magn. Reson. Med 2012;68:863–867. [PubMed: 22162033]
30. Haacke EM, Brown RW, Thompson MR, Venkatesan R. Magnetic resonance imaging: physical principles and sequence design. Wiley-Liss New York:; 1999.
31. Robinson S, Grabner G, Witoszynskyj S, Trattnig S. Combining phase images from multi-channel RF coils using 3D phase offset maps derived from a dual-echo scan. Magn. Reson. Med 2011;65:1638–1648. [PubMed: 21254207]
32. Gudbjartsson H, Patz S. The Rician Distribution of Noisy MRI Data. Magn. Reson. Med. 1995;34:910–914. [PubMed: 8598820]
33. Sprinkhuizen SM, Konings MK, van der Bom MJ, Viergever MA, Bakker CJG, Bartels LW. Temperature-induced tissue susceptibility changes lead to significant temperature errors in PRFS-based MR thermometry during thermal interventions. Magn. Reson. Med. 2010;64:1360–1372. [PubMed: 20648685]
34. Maurer HS, Behrman RE, Honig GR. Dependence of the Oxygen Affinity of Blood on the Presence of Foetal or Adult Haemoglobin. Nature 1970;227:388–390. [PubMed: 5428441]

35. Becklake MR, Griffiths SB, McGregor M, Goldman HI, Schreve JP. Oxygen dissociation curves in sickle cell anemia and in subjects with the sickle cell trait. J. Clin. Invest. 1955;34:751–755. [PubMed: 14367534]

36. Dash RK, Korman B, Bassingthwaighte JB. Simple Accurate Mathematical Models of Blood HbO2 and HbCO2 Dissociation Curves at Varied Physiological Conditions–Evaluation and Comparison with other Models. Eur. J. Appl. Physiol 2016;116:97–113.

37. Wagner MH, Berry RB. A Patient With Sickle Cell Disease and a Low Baseline Sleeping Oxygen Saturation. J. Clin. Sleep Med. JCSM Off. Publ. Am. Acad. Sleep Med 2007;3:313–315.

38. Yablonskiy DA, Haacke EM. Theory of NMR signal behavior in magnetically inhomogeneous tissues: the static dephasing regime. Magn. Reson. Med 1994;32:749–763. [PubMed: 7869897]

39. Young RC, Rachal RE, Del Pilar Aguinaga M, et al. Automated oxyhemoglobin dissociation curve construction to assess sickle cell anemia therapy. J. Natl. Med. Assoc 2000;92:430–435. [PubMed: 11052456]

40. Benesch R, Benesch RE. The effect of organic phosphates from the human erythrocyte on the allosteric properties of hemoglobin. Biochem. Biophys. Res. Commun 1967;26:162–167. [PubMed: 6030262]

41. Chanutin A, Curnish RR. Effect of organic and inorganic phosphates on the oxygen equilibrium of human erythrocytes. Arch. Biochem. Biophys 1967;121:96–102. [PubMed: 6035074]

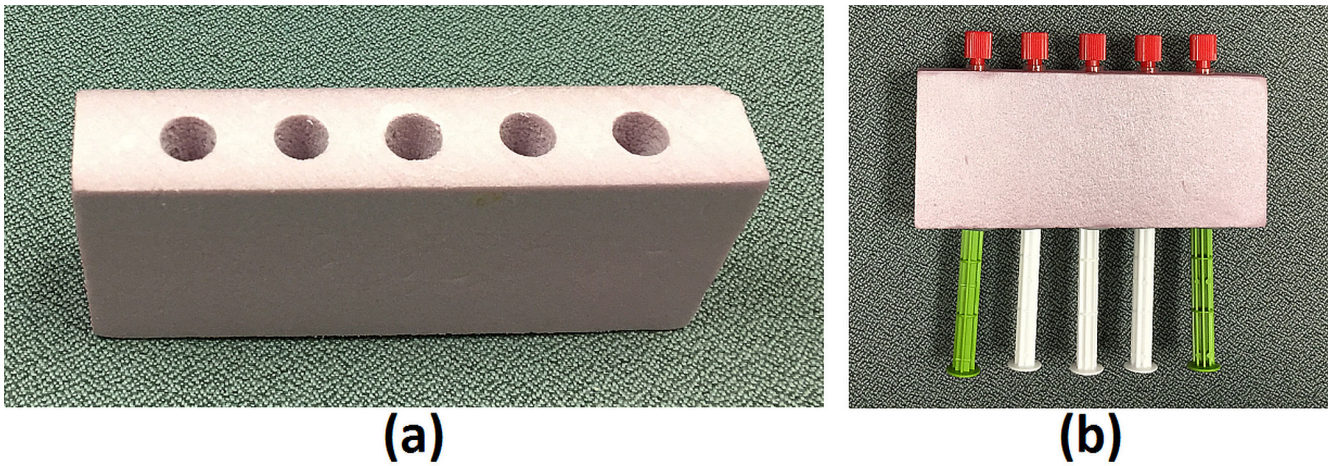

Figure 1 –.
Custom holder with (a) no syringes, (b) with syringes. The blood sample was always placed at the central holder.

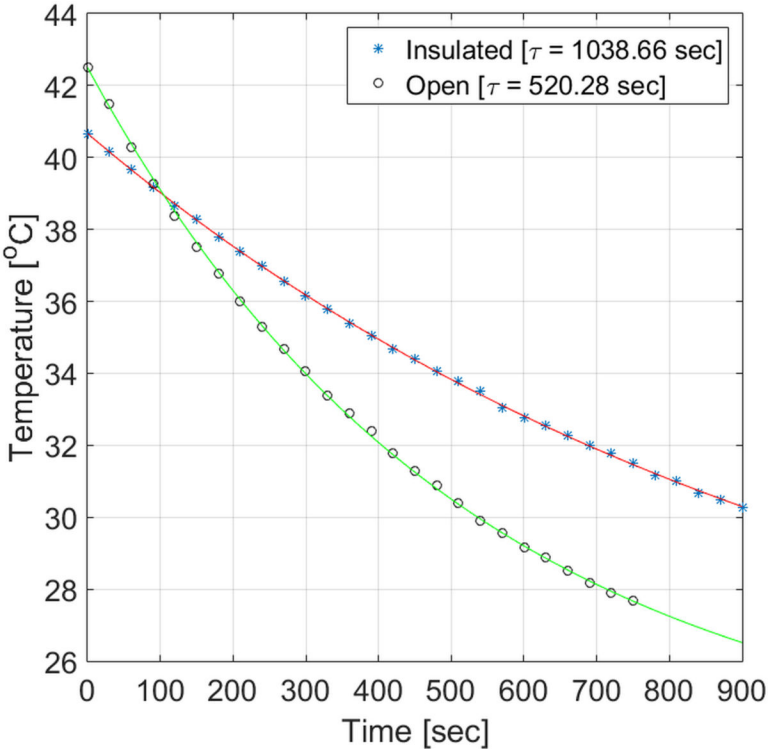

Figure 2 –.
Temperature decrease for samples placed inside or outside the custom holder.

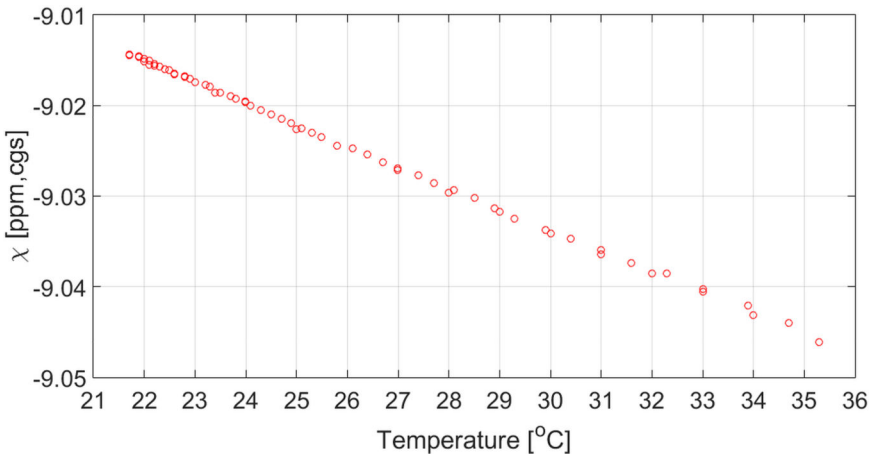

Figure 3 –.
Bulk volume susceptibility as a function of temperature over the experimental range.

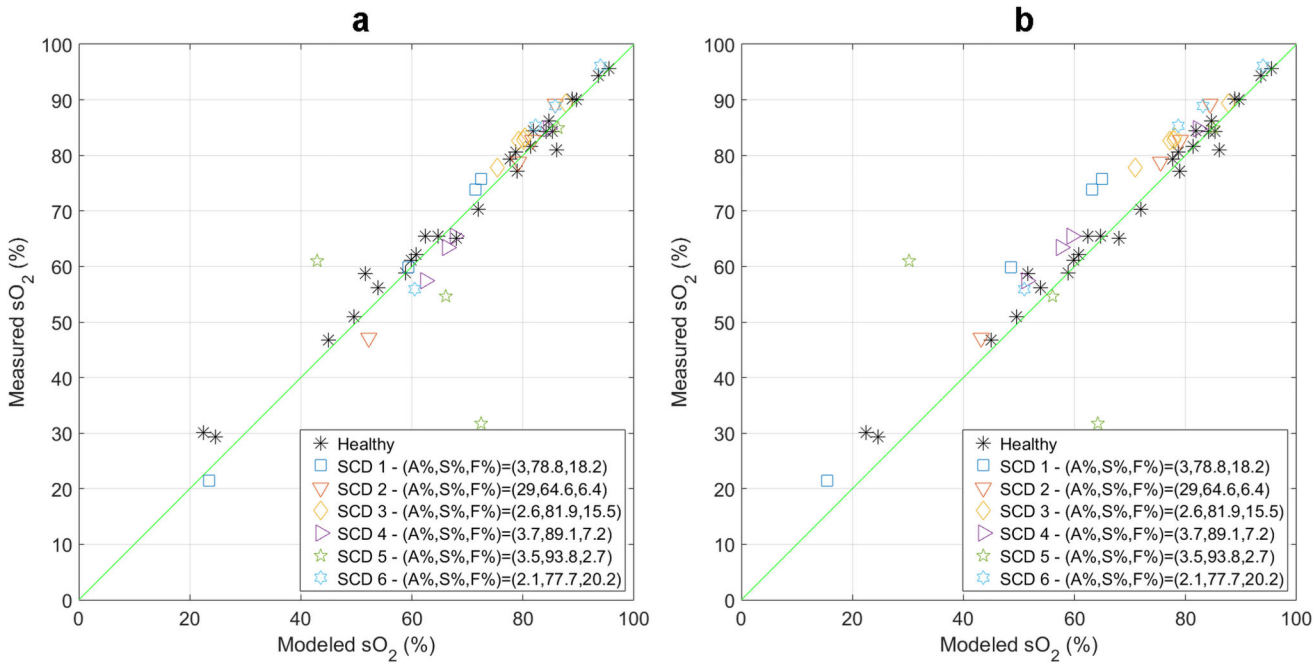

Figure 4 –.

Modeled (weighted sum) vs. measured oxygen saturation percentages using (a) the DBM model and (b) the DWM model. The green line is the line of identity.

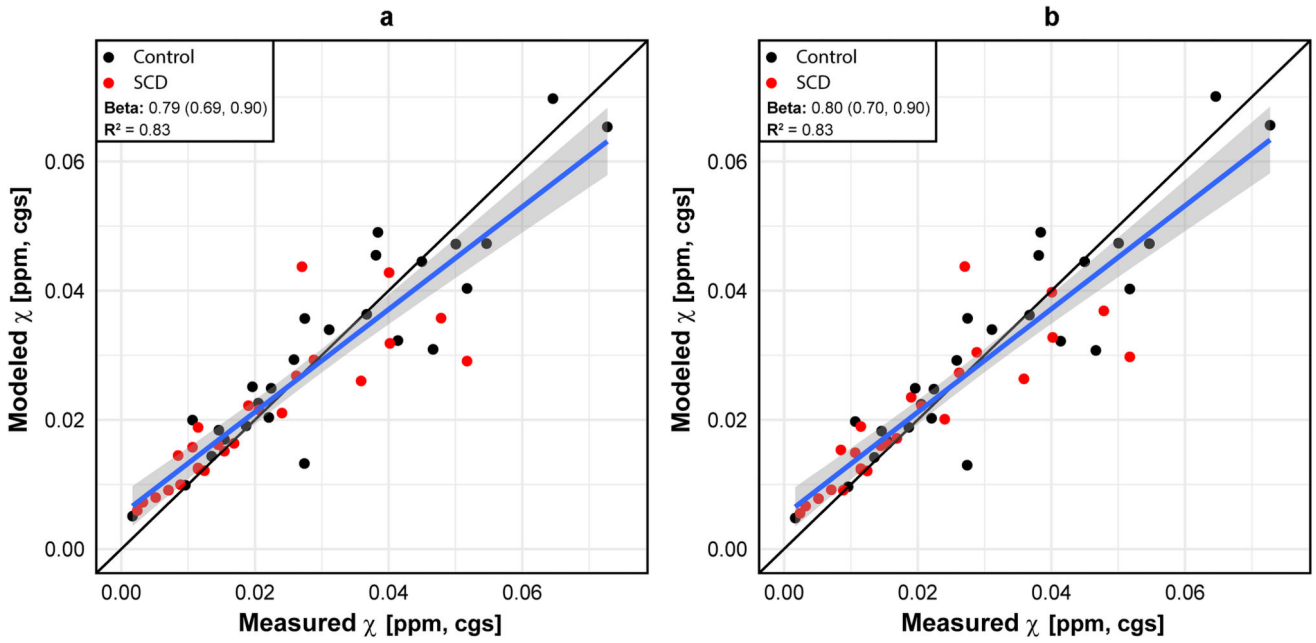

Figure 5 –.

Modeled vs measured susceptibilities using the reduced model (Equation 4) based on (a) the DBM model and (b) the DWM model.

Table 1 –

Blood analysis from healthy and SCA participants. The baseline %SpO2 was the average SpO2 in the year prior to this study.

	Age (y)	Gender	Baseline %SpO_2	%Hct	%HbA	%HbS	%HbF	%MetHb	%COHb	pH Range
Controls	33	F	N/A	40.4	100	0	0	0.9	0.8	7.18–7.36
	52	M	N/A	42.6	100	0	0	1	1	7.22–7.38
	40	F	N/A	38.7	100	0	0	1	1.2	7.18–7.51
	45	M	N/A	42.5	100	0	0	0.7	0.7	7.31–7.42
	35	M	N/A	41.6	100	0	0	0.8	1.1	7.30–7.39
	24	M	N/A	42.5	100	0	0	1.8	1	7.36–7.40
μ±σ	**38.2±9.8**	-		**41.4±1.6**	**100±0**	**0±0**	**0±0**	**1±0.4**	**1±0.2**	-
SCA	41	F	98.7	21.7	3	78.8	18.2	1.7	3.5	7.33–7.36
	39	M	88.5	18	29	64.6	6.4	2.8	5	7.32–7.38
	25	M	95.3	29.7	2.6	81.9	15.5	3.4	10.1	7.42–7.47
	22	F	97.0	22	3.7	89.1	7.2	3.1	3.2	7.30–7.39
	25	F	95.7	19.2	3.5	93.8	2.7	1.8	4.5	7.26–7.39
	18	M	96.5	28.5	2.1	77.7	20.2	1.4	3.6	7.27–7.44
μ±σ	**28.3±9.4**	-	**95.3±3.5**	**23.2±4.8***	**7.3±10.6***	**81±10.1***	**11.7±7.2***	**2.4±0.8***	**5±2.6***	-

Magn Reson Med. Author manuscript; available in PMC 2022 June 01.